Graphitic-Phase C3N4 Nanosheets Combined with MnO2 Nanosheets for Sensitive Fluorescence Quenching Detection of Parathion-Methyl

Bicheng Liu
  Nanchang University - Qianhu Campus: Nanchang University

Sihao Wu
  Nanchang University - Qianhu Campus: Nanchang University

Zoujun Peng
  Nanchang University - Qianhu Campus: Nanchang University

Jiahan Rui
  Nanchang University - Qianhu Campus: Nanchang University

Ping Qiu (✉ pingqiu@ncu.edu.cn)
  Nanchang University - Qianhu Campus: Nanchang University   https://orcid.org/0000-0003-1680-6378

Abstract

In this study, we have developed a sensitive approach to measure organophosphorus pesticides (OPs) using graphitic-phase C_3N_4 nanosheets (g-C_3N_4) combined with a nanomaterial-based quencher MnO_2 nanosheets (MnO_2 NS). Because MnO_2 NS could quench the fluorescence of g-C_3N_4 via the inner-filter effect (IFE), the enzymatic hydrolysate (thiocholine, TCh) can efficiently trigger the decomposition of MnO_2 nanosheets in the presence of acetylcholinesterase (AChE) and acetylthiocholine, resulting in the fluorescence recovery of g-C_3N_4. OPs, as inhibitors for AChE activity, can prevent the generation of TCh and decomposition of MnO_2 nanosheets, accompanied by fluorescence quenching again. So the AChE-ATCh-MnO_2-g-C_3N_4 system can be utilized to detect OPs quantitatively based on the g-C_3N_4 fluorescence. Under the optimum conditions, the linear range for the determination of parathion-methyl (PM) and 2,2-dichlorovinyl dimethyl phosphate (DDVP) were found in the range of 0.1-2.1 ng/mL with a limit of detection of 0.069 ng/mL, and 0.5-16 ng/mL with a limit of detection of 0.069 ng/mL, respectively. Finally, this method was exploited for the monitoring of PM in real samples. The advantages of the assay are user-friendly, easy-to-ease, cost-effective compared to sophisticated analytical instruments.

Introduction

The development of agricultural industrialization makes agricultural products more and more dependent on pesticides. As China is a large agricultural country in development, the consumption of pesticides is increasing day by day. However, the chronically, continuously, and largely absurd application of pesticides results in many typical cases of negative environmental consequences [1, 2]. Organophosphorus pesticides (OPs) are anti acetylcholinesterase (AChE) and act via a common mechanism of phosphorylation of AChE, which disables AChE to catalyze acetylcholine and results in over-accumulation of acetylcholine leading into cholinergic toxicity [3, 4]. OPs are one of the main causes of acute pesticide poisoning and they are also the key pesticide residues in fruits and vegetables. OPs can cause chronic poisoning, long-term contact, or food containing pesticide residues, and make pesticide accumulation in the body, cause physiological barriers, and also can affect the reproductive system, cause fetal malformation. Some pesticides have obvious carcinogenicity and mutagenicity [5]. More people pay attention to all kinds of problems which are caused by pesticide residues.

There are several analytical techniques reported for the determination of OPs from a variety of samples, including liquid/gas- mass spectrometry (LC/GC-MS), high performance liquid chromatography (HPLC), electrochemical method, and enzyme-linked immunoassay [6−9]. However, the existing detection methods are time-consuming, costly complicated with related equipment conditions, and require specially well-trained personnel to operate [10]. Fluorescence technology is found to be highly sensitive, simple, low cost, and low detection limit for the determination of OPs by using the fluorescent probe [11, 12]. Yan et al. developed a novel Fe_3O_4 magnetic nanoparticle (MNP) peroxidase mimetic-based colorimetric method for the rapid detection of OPs and nerve agents [13]. A highly sensitive, rhodamine B-covered gold nanoparticle (RB-AuNP) -based assay with dual readouts (colorimetric and fluorometric) for detecting

organophosphorus and carbamate pesticides in complex solutions was reported [14]. A simple and sensitive fluorescent sensor based on l-tyrosine methyl ester functionalized carbon dots (Tyr-CDs) and tyrosinase system was proposed for methyl parathion [15].

Some common fluorescent materials, such as carbon nanomaterials,were prepared with hydrothermal method and must be extensively dialyzed for three days, which was time consuming and leading to a quite low yield (milligram level) [16]. Graphitic-phase C_3N_4 nanosheets (g-C_3N_4) is easily-prepared via one-step polymerization of cheap feedstocks like cyanamide, urea, thiourea, melamine, and dicyandiamide. It possesses a unique two-dimensional layered graphite-like structure composed of carbon and nitrogen atoms and has some advantages such as excellent chemical stability and tunable electronic structure [17, 18]. g-C_3N_4 is not only economical and environmentally friendly but also possesses excellent physicochemical properties. The characteristics of g-C_3N_4 include high fluorescence quantum yields, heavy-metal free structure, high biocompatibility, and low toxicity, which made it so hot [19]. g-C_3N_4 as fluorophores has been applied to detect all kinds of anions, metal ions, and bio thiols [20–22].

MnO_2 NS is a kind of novel, facile-synthesized 2D nanomaterial with good biocompatibility, single-layer manganese dioxide nanosheet [23]. It was reported MnO_2 NS possess oxidase-like property. They that can react with thiocholine (TCh, a hydrolyzed product of acetylthiocholine) and reduced to Mn^{2+} by TCh [24, 25]. Furthermore, it is interesting that MnO_2 NS can quench many fluorophores including g-C_3N_4 through inner filter effect (IFE) [26].

As we all know, the activity of acetylcholinesterase is inhibited in the presence of OPs, so the hydrolysis of acetylcholine is inhibited. The reaction of hydrolysis product (TCh) with MnO_2 NS is also limited directly, which determines the degree of fluorescence recovery of g-C_3N_4. The fluorescence intensity of g-C3N4 recovers proportionally with the concentration of PM. So we designed a sensitive fluorescent assay to detect parathion-methyl using g-C_3N_4 probe with MnO_2 nanosheets.

Experiments

Materials and reagents

Parathion-methyl (PM) was purchased from the Nation Institute of Metrology (Beijing, China) and was used without further purification. The standard solution of PM (0.01 mg/mL) was prepared by dissolving in methanol. Tetramethylammonium hydroxide and Tris (hydroxymethyl) methyl aminomethane were purchased from Adamas-beta Reagent Company (Shanghai, China), and manganese chloride ($MnCl_2$) were obtained from Sinopharm Chemical Reagent Company (Shanghai, China). Melamine and hydrogen peroxide (H_2O_2) were purchased from Aladdin Industrial Corporation (Shanghai, China). Acetylcholinesterase (AChE, 744 unit/mg) and acetylthiocholine iodide (ATCh) were purchased from Sigma-Aldrich (Shanghai, China). The buffer solutions used in this study were as follows: Phosphate buffer (PB) (pH 5; 25 mM); Phosphate buffer solution (PBS) (pH 8.5; 10 mM); Tris-HCl buffer (pH 7.5;

20 mM) was used to dissolve the AChE (1 unit/mL). The solution of ATCh (10 mmol/L) was freshly prepared in ultrapure water and used within 3 h. All chemicals were of analytical-reagent grade, and the ultrapure water (18.25 MΩ, Millipore, USA) was used throughout the experiments.

Instrumentation

UV-vis Absorption spectra were recorded using UV-2450 Shi-madzu Vis-spectrometer (Japan), the fluorescence spectra were collected on an F-4600 fluorescence spectrometer (Hitachi, Japan). The morphology of the MnO_2 NS was characterized by transmission electron microscopy (TEM, JEM-2100, JEOL Co., Japan) operating at 200 kV acceleration voltage. X-ray photoelectron spectroscopy (XPS) was carried out on Esca Lab 250Xi with Al K α X-ray radiation as the source for excitation. The crystalline structure of the nanoflakes was investigated by X-ray diffraction (XRD, Bruker, Germany) with the scanning speed of 2°/min. Scanning electron microscopy (SEM) images were obtained with a JSM-6701F microscope system (JEOL Co., Tokyo, Japan). Zeta potentials were obtained using a Nano ZS90 (Malvern, UK). The binding energies were calibrated by C 1 s (284.8 eV), and pass energy was 30.0 eV with a spot size of 650 μm. The sample for TEM characterization was prepared by placing a drop of the MnO_2 NS solution on a carbon-coated copper grid and drying it at room temperature.

Synthesis of MnO_2 nanosheets

MnO_2 NS was synthesized by a simple wet chemical method [27]. For this, 10 mL tetramethylammonium hydroxide (6%) was added to 30 mL of H_2O_2 (3%), then 20 mL of $MnCl_2$ (0.3 M) was quickly transferred into the above solution within 15 s. The color of the mixture solution quickly turned dark brown, and the mixture was kept on stirring for 12 h at room temperature. After stirring, the obtained mixture was centrifuged at 4000 rpm for 30 min and washed successively with ultrapure water and methanol. Next, the bulk MnO_2 NS was dried at 60 °C for 72 h. 0.0030 g of MnO_2 NS was dissolved in 60 ml of water, and brown MnO_2 NS dispersion was obtained after sonication for 12 h, which was stored in a refrigerator at 4 °C for further experiments.

Preparation of g-C_3N_4

g-C_3N_4 was synthesized by the direct thermal treatment of melamine as reported in previous work [28]. An alumina crucible with a cover, contained melamine (10 g) was heated to 600 °C with a heating rate of 3 °C/min under air conditions, and was kept at that temperature for 2 h. Cooling the product to room temperature, the yellow g-C_3N_4 powder was obtained. 0.0080 g of powder yellow g-C_3N_4 product was dissolved in 10 ml of water, which was stored in a refrigerator at 4 °C for further experiments.

Fluorescence method for detection of PM

AChE (50 μL,100 U/L) contained a series of different concentrations (10 μL) of PM were added to centrifuge tubes and incubated at 37 °C for 0.5 h. ATCh (5 mM, 40 μL), MnO_2 NS (30 μg/mL, 100 μL) and PBS buffer (200 μL, pH 7) were added successively to centrifuge tubes and incubated at 37 °C for another 0.5 h. Then, g-C_3N_4 (100 μL, 0.8 mg/mL) was mixed to the reaction system and diluted the final volume

of 2000 μL. The fluorescence emission spectrum was measured, and the fluorescence intensity at 460 nm was recorded.
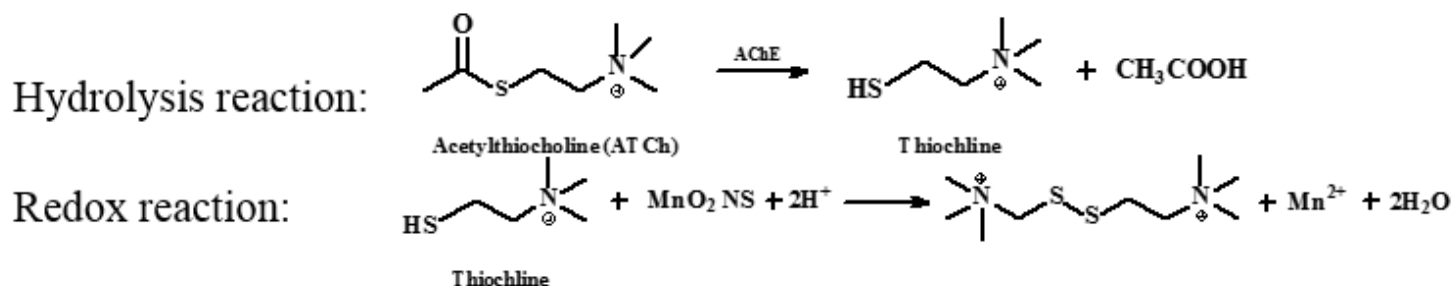
Results And Discussion

Characterization of MnO_2 NS and g-C_3N_4

Firstly, MnO_2 NS was characterized by transmission electron microscopy (TEM), which showed a two-dimensional structure, and exhibited multiple folds and crinkles in Fig. 1a. Meanwhile, MnO_2 NS had a wide UV absorption band ranging from 300 nm to 600 nm, and the maximum absorption was concentrated at 360 nm (Fig. 1b). Detailed analysis based on Xray photoelectron spectroscopy (XPS) was further investigated to confirm the features of MnO_2 NS. Figure 1c displayed the XPS spectrum for the MnO_2 NS. The two peaks of the $Mn2p_{3/2}$ and $Mn2p_{1/2}$ located at 642.0 and 653.9 eV were detected and was proved to be attributed to Mn^{2+} [29, 30]. Thus, the above characterization indicated that MnO_2 NS had been synthesized successfully.

On the other hand, the morphologies of g-C_3N_4 nanocomposites was carried out using SEM, XRD and XPS in details. Figure 1d showed the SEM images of g-C_3N_4, which investigated the microstructure of g-C_3N_4. The surface of g-C_3N_4 has loose aperture and rough block structure. XRD patterns were used to identify the crystal structure of g-C_3N_4 and the resultshowed a major diffraction peak occurred at around 27.3⬜ as shown in Fig. 1e. No diffraction peaks of other impurity phases were detected in all the samples. The strong peak at around 27.3⬜ could be indexed as (002), which was due to interplanar stacking of aromatic systems[31]. The typical XPS survey scan is an effective way to investigate the chemical bonding environment and the states of elements in g-C_3N_4 nanocomposites. As shown in Fig. 1f, the complete survey XPS spectrum reveals that C and N peaks could be found in all samples, and no peaks of other elements were observed, indicating that the g-C_3N_4 nanocomposites kept the same chemical composition and chemical states [31].

Principle of fluorescence sensing strategy

In the system, it is interesting that MnO_2 NS acts not onlyas the quencher of g-C3N4, but also as as an oxidizing agent of TCh. g-C_3N_4 exhibited a strong fluorescence emission, but MnO_2 NS could quench the fluorescence of g-C_3N_4 at 460 nm via the inner-filter effect (IFE). As shown in scheme 1, ATCh was catalyzed by AChE and hydrolyze to form TCh and acetic acid. A redox reaction occurred between sulfhydryl group (-SH) of TCh with MnO_2 NS to form disulfide (-S-S-) and Mn^{2+}, resulting in the fluorescence recovery of g-C_3N_4. OPs, as inhibitors for AChE activity, can prevent the generation of TCh and decomposition of MnO_2 nanosheets, accompanied by fluorescence quenching again. So the AChE-ATCh-MnO_2-g-C_3N_4 system can be utilized to detect OPs quantitatively based on the g-C_3N_4 fluorescence.

Hydrolysis reaction:

Acetylthiocholine (ATCh) → Thiochline + CH₃COOH (via AChE)

Redox reaction:

Thiochline + MnO₂ NS + 2H⁺ → disulfide + Mn²⁺ + 2H₂O

To verify the detection mechamism of fluorescence sensing strategy, Fig. 2a shows UV-vis absorption spectrum of MnO$_2$ NS and the mixture with AChE and ATCh. MnO$_2$ NS have a obvious UV absorption peak located at 360 nm (Fig. 2a) [27]. In addion, it was found that the color of MnO$_2$ NS itself was yellow, but it became pale in the presence of AChE and ATCh (the inset images of Fig. 2a), and the absorption peaks of MnO$_2$ NS also decreased. As described previously, ATCh is hydrolyzed to form TCh and acetic acid hydrolyzing by AChE. We can conclude that redox reaction occurred between sulfhydryl group (-SH) of TCh with MnO$_2$ NS to form disulfide (-S-S-) and Mn^{2+}, which can restore the fluorescence of g-C3N4 at 460 nm. Figure 2b show the spectra of g-C3N4 and the mixture with different substances, and it was found that the fluorescence intensity of g-C3N4 was different significantly. In Fig. b (1), (2), (3), they had similar fluorescence intensity, which showed that both AChE and ATCh have no effect on the fluorescence intensity of g-C3N4. In Fig. b (5) the weak fluorescence was observed, which illustrated that MnO$_2$ NS would quench the fluorescence of g-C3N4 strongly. Compared the curve 3 with curve 5, the fluorescence intensity of g-C3N4 be restored in the presence of AChE and ATCh. It is because that TCh reduced MnO$_2$ NS to Mn^{2+}, which caused the decrease of MnO$_2$ NS in the system and the fluorescence intensity of g-C3N4 restored. Compared curve 3 with curve 4, there was less TCh to react with MnO$_2$ NS with the existence of PM, so the fluorescence of g-C3N4 was still quenched again. The mechanism of quenching fluorescence by MnO$_2$ NS includes fluorescence resonance energy transfer (FRET) and inner-filter effect (IFE). To further explore the quenching mechanism of MnO$_2$ NS on g-C3N4, the zeta potential and UV-vis absorption spectrum were carried out. As shown in Fig. 2c, the zeta potentials of g-C3N4, MnO$_2$ NS, and the mixture are all negatively charged, so there is electrostatic repulsion between g-C3N4 and MnO$_2$ NS. It demonstrated that g-C3N4 and MnO$_2$ NS could not be close to produce fluorescence resonance energy transfer. On the other hand, Fig. 2d showed the fluorescence emission spectra of g-C3N4 and the UV-vis absorption spectra of the MnO$_2$ NS. It can be seen that there was a strong overlap between the emission spectrum and the absorption spectrum, which provided the necessary condition for the inner filter effect (IFE). The above results show that MnO$_2$ NS quenches the fluorescence of g-C$_3$N$_4$ through IFE.

Optimization of the detection conditions for fluorescence analysis

To obtain the optimal fluorescence sensing response for the detection of PM using g-C3N4/MnO$_2$ NS, the experimental parameters affecting sensitivity and selectivity were all optimized, including the

concentrations of AChE, MnO$_2$ NS and g-C3N4, pH, the reaction time, and the concentration of ATCh.

For this, the relative intensity was used to evaluate the optimal reaction system, which can be represented by (F$_0$-F)/F$_0$. Herein, F$_0$ is the fluorescence intensity of g-C3N4, and F is the fluorescence intensity after the redox reaction. As shown in Fig. 3a, the sensitivity increased slowly with the increase of AChE content and the maximum sensitivity was obtained when the concentration of AChE was 250 U/L. The effect of the concentrations of MnO$_2$ NS (15–40 μg/mL) and g-C3N4 (5–80 μg/mL) on relative intensities were both investigated respectively (Fig. 3b and 3c). It can be concluded that the optimal concentrations of MnO$_2$ NS and g-C3N4 were 30 μg/mL and 60 μg/mL, respectively. Next, it was found that the maximum sensitivity was obtained when the pH was 7 (Fig. 3d). Figure 3e showed the influence of oxidation time of probe pairs and the sensitivity reached the stable performance at 30 minutes. The concentration of ATCh could effect the degree of oxidation reaction of MnO$_2$ NS (Fig. 3f), and the higher the concentration is, the more complete the reaction was. The relative intensity kept stable after 3 mM ATCh.

Linearity and limit of detection

PM and DDVP were chosen as typical OPs for the detection based on g-C3N4/ MnO$_2$ NS. Under optimum experimental conditions, a range of their concentrations for detection was investigated as shown in Fig. 4. According to the detection principle, a fluorescence quenching takes place with the addition of OPs and the degree of fluorescence quenching is proportional to their concentrations. The linear range of PM concentration was obtained from 0.1 to 2.1 ng/mL (Fig. 4a). The inset indicated a good fit to the linear model, and the obtained linear least square equation was expressed as Y = -246.2X + 1509 (ng/mL) with the correlation coefficient (R^2) of 0.993. The limit of detection (LOD) was calculated to be 0.069 ng/mL according to LOD = 3σ/k, where σ stands for standard-error of estimate and k is the slope of linear-regression-line. For DDVP, the linear regression equation was Y = -53.9X + 1317.2 (ng/mL) with the correlation coefficient (R^2) of 0.995 and the LOD was 0.20 ng/mL (Fig. 4b). LOD and linear range of this assay was compared with the already reported methods, and the comparison is presented in Table 1 [32–36], the fluorescent assay for the determination of OPs based on g-C3N4/MnO$_2$ NS/AChE-ATCh fluorescent probes has higher sensitivity and excellent analytical performance.

Table 1 Comparison of the proposed assay with other reported methods for the detection of pesticides

Sample	Target	LOD	Linear range	Ref.
TPE-1, TPE-2	dimethoate	0.008 mg/L	0.009−22.5 mg/L	[32]
upconversion nanoparticles	chlorpyrifos	6.7 ng/mL	20-2000 ng/mL	[33]
$CsPbBr_3$ QDs	phoxim	1.45 ng/mL	5-100 ng/mL	[34]
copper	dichlorvos	0.97 ng/mL	1−2 ng/mL	[35]
C-dots	chlorpyrifos	3 ng/ mL	0.01-1.0 ng/mL	[36]
MnO_2 NS- $g-C_3N_4$	PM	0.069 ng/mL	0.1−2.1 ng/mL	This work

Test of selectivity

To test the selectivity of the assay, the control experiment was performed based on several potential interfering ions in practical samples, including metal ions (Na^+, K^+, Ca^{2+}, and Mg^{2+}), anions (Cl^-, SO_4^{2-}, CO_3^{2-} and PO_4^{3-}), and biomolecules (Vitamin B (V_B), glycine and tyrosine, humic acids, chlorophyll). We added the interfering substances to the reaction system in the presence of PM (1 ng/mL), and their final concentrations were 100 times the standard concentration of PM. Compared to the control group, the relative change varied from 0.91 to 1.1, so there is no significant difference (Fig. 5).Therefore, the developed g-C3N4/ MnO_2 NS based fluorescence assay was specific for OPs detection and can be applied for PM determination in these common substances do not interfere with the assay with high selectivity.

Real samples detection

OPs often processes into the lake with watering, rainfall, and other. So Lake water samples were collected as real samples from Longteng Lake and Qian Lake in Nanchang city, China. Water samples were spiked with PM to get that desired concentration and then were pretreated according to the method reported in the previous literature[37]. The collected samples were filtered through a 0.45 μm membrane syringe filter to remove any particulate matter. As summarized in Table 1, the recovery (recovery rate (%) = $100×(C_{detection\ amount}/C_{addition\ amount})$) for PM of the proposed methods for two samples was in the range of 85.2-116.9% and 82.2-109.6%, with RSD ($n = 3$) for less than 3.4% and 4.2%, respectively. The results demonstrated that the proposed methods could be applied to detect PM in practical samples.

Table 1 PM detection in two real lake water samples

Sample	Added (ng/mL)	Found (ng/mL)	Recovery (%)	RSD (%)
Longteng Lake	0	0	0	0
	5	4.26	85.2	3.4
	10	11.69	116.9	2.2
	20	21.1	105.5	1.9
Qian Lake	0	0	0	0
	5	4.58	91.6	4.2
	10	8.22	82.2	3.9
	20	21.92	109.6	2.8

Conclusions

In this study, we developed a convenient, reliable, and sensitive assay for OPs detection based on MnO_2 NS/g-C_3N_4. The g-C_3N_4 were employed as the fluorescence units, and the MnO_2 nanosheets were used as the dual-functional nanoquencher and oxidizing agent in this developed platform. The strategy depends on TCh decomposition of MnO_2 nanosheets and OPs-caused inhibition of the enzyme. The proposed method shows sensitivity and high-selectivity towards PM, and the limit of detection reaches as low as 0.069 ng/mL. The present assay shows many advantages including environmental-friendliness, cost-effectiveness, and ease-of-use, demonstrating that the convenient strategy could serve as a promising platform for detecting OPs.

Declarations

Authors' Contributions All authors contributed in the present study. All authors commented on this version of the manuscript and they read and approved the final manuscript.

Availability of Data and Materials Not applicable.

Compliance with Ethical Standards

Competing Interests Authors declare that they have no conflict of interst.

References

[1] Jin JJ, Wang WY, He R, Gong HZ (2017) Pesticide use and risk perceptions among small-scale farmers in anqiu county. Int J Environ Res Public Health 14:29-38

[2] Zhou JH, Jin SS (2009) Safety of vegetables and the use of pesticides by farmers in China: Evidence from Zhejiang province. Food Control 20:1043-1048

[3] Damalas CA, Eleftherohorinos IG (2011) Pesticide Exposure, Safety Issues, and Risk Assessment Indicators. Int J Environ Res Public Health 8:1402-1419

[4] Pohanka M, Drtinova L, Kuca K (2012) Acetylcholinesterase based assay of eleven organophosphorus pesticides: finding of assay limitations. Int J Environ Anal Chem 92:125-132

[5] Li BX, Wang A (2015) A review on the toxicity of pyrethroid pesticides and their harms to population health. Asian J Ecotoxicol 10:29-34

[6] Louter AJH, Hogenboom AC, Slobodnik J, Vreuls RJJ, Brinkman UAT (1997) Use of chemical ionization in multianalysis gas and liquid chromatography combined with a single mass spectrometer for the ultra-trace level determination of microcontaminants in aqueous samples. Analyst 122:1497-1503

[7] Chen HX, Chen H, Ying J, Huang JL, Liao L (2009) Dispersive liquid-liquid microextraction followed by high-performance liquid chromatography as an efficient and sensitive technique for simultaneous determination of chloramphenicol and thiamphenicol in honey. Anal Chim Acta 632:80-85

[8] Liu GD, Lin YH (2006) Biosensor based on self-assembling acetylcholinesterase on carbon nanotubes for flow injection/amperometric detection of organophosphate pesticides and nerve agents. Anal. Chem 78:835-843

[9] Qian GL, Wang LM, Wu YR, Zhang Q, Sun Q, Liu Y, et al (2009) A monoclonal antibody-based sensitive enzyme-linked immunosorbent assay (ELISA) for the analysis of the organophosphorous pesticides chlorpyrifos-methyl in real samples. Food Chem 117:364-370

[10] Pundir CS, Chauhan N (2012) Acetylcholinesterase inhibition-based biosensors for pesticide determination: A review. Anal Biochem 429:19-31

[11] Liu DB, Chen WW, Wei JH, Li XB, Wang Z, Jiang XY (2012) A highly sensitive, dual-readout assay based on gold nanoparticles for organophosphorus and carbamate pesticides. Anal Chem 84:4185-4191

[12] Zhang K, Mei QS, Guan GJ, Liu BH, Wang SH, Zhang ZP (2010) Ligand replacement-induced fluorescence switch of quantum dots for ultrasensitive detection of organophosphorothioate pesticides. Anal Chem 82:9579-9586

[13] Liang MM, Fan KL, Pan Y, Jiang H, Wang F, Yang DL, et al (2013) Fe_3O_4 magnetic nanoparticle peroxidase mimetic-based colorimetric assay for the rapid detection of organophosphorus pesticide and nerve agent. Anal Chem 85:308-312

[14] Tan KJ, Li JY, Li HC, Wang YY, Yuan R (2014) A highly sensitive dual-readout assay based on poly(A) and gold nanoparticles for palmatine hydrochloride. Spectrochim Acta A 122:198-203

[15] Hou JY, Dong J, Zhu HS, Teng X, Ai SY, Mang ML (2015) A simple and sensitive fluorescent sensor for methyl parathion based on l -tyrosine methyl ester functionalized carbon dots. Biosens Bioelectron 68:20-26

[16] Xie HZ, Feng B, Hou JY, Ai SY (2018) A highly sensitive dual-signaling assay via inner filter effect between g-C$_3$N$_4$ and gold nanoparticles for organophosphorus pesticides. Sensor Actuat B-Chem 255:2232-2239

[17] Zhao ZW, Sun YJ, Dong F (2015) Graphitic carbon nitride based nanocomposites: a review. Nanoscale 7:15-37

[18] Chu X, Li K, Guo HY, Zheng HB, Shuda S, Wang XL, et al (2017) Exploration of graphitic-C$_3$N$_4$ quantum dots for microwave-induced photodynamic therapy. ACS Biomater Sci Eng 3:1836-1844

[19] Cheng Q, Liu XY, He Y, Ge YL, Zhou JG, Song GW (2019) Fabrication of fluorescence turn-off-on sensor based on g-C$_3$N$_4$ quantum dots and MgFe layered double hydroxide for the detection of citrate. J Fluoresc 29:719-726

[20] Zhang XL, Zheng C, Guo SS, Li J, Yang HH, Chen GN (2014) Turn-On fluorescence sensor for intracellular imaging of glutathione using g-C$_3$N$_4$ nanosheet-MnO$_2$ sandwich nanocomposite. Anal Chem 86:3426-3434

[21] Liu JW, Luo Y, Wang YM, Duan LY, Jiang JH, Yu RQ (2016) Graphitic carbon nitride nanosheets-based ratiometric fluorescent probe for highly sensitive detection of H$_2$O$_2$ and glucose. ACS Appl Mater Inter 8:33439-33445

[22] Cheng NY, Jiang P, Liu Q, Tian JQ, Asiri AM, Sun XP (2014) Graphitic carbon nitride nanosheets: one-step, high-yield synthesis and application for Cu^{2+} detection. Analyst 139:5065-2068

[23] Dong ZZ, Lu LH, Ko CN, Yang C, Li SN, Lee MY, et al (2017) A MnO$_2$ nanosheet-assisted GSH detection platform using an iridium(III) complex as a switch-on luminescent probe. Nanoscale 9:4677-4682

[24] Yan X, Song Y, Wu XL, Zhu CZ, Su XG, Du D, et al (2017) Oxidase-mimicking activity of ultrathin MnO$_2$ nanosheets in colorimetric assay of acetylcholinesterase activity. Nanoscale 9:2317-2323

[25] Deng JJ, Lu DK, Zhang XL, Shi GY, Zhou TS (2017) Highly sensitive GQDs-MnO$_2$ based assay with turn-on fluorescence for monitoring cerebrospinal acetylcholinesterase fluctuation: A biomarker for organophosphorus pesticides poisoning and management. Environ Pollut 224:436-444

[26] Fan DQ, Shang CS, Gu WL, Wang EK, Dong SJ (2017) Introducing ratiometric fluorescence to MnO_2 nanosheet-based biosensing: A simple, label-free ratiometric fluorescent sensor programmed by cascade logic circuit for ultrasensitive GSH detection. ACS Appl Mater Inter 9:25870-25877

[27] Yao TT, Liu AR, Liu Y, Wei M, Wei W, Liu SQ (2019) Ratiometric fluorescence sensor for organophosphorus pesticide detection based on opposite responses of two fluorescence reagents to MnO_2 nanosheets. Biosens Bioelectron 145:111705

[28] Tian JQ, Liu Q, Asiri AM, Qusti AH, Al-Youbi AO, Sun XP (2013) Ultrathin graphitic carbon nitride nanosheets: a novel peroxidase mimetic, Fe doping-mediated catalytic performance enhancement and application to rapid, highly sensitive optical detection of glucose. Nanoscale 5:11604-11609

[29] Wang S, Wang L, Xu XW, Li X, Jiang W (2019) MnO_2 nanosheet-mediated ratiometric fluorescence biosensor for MicroRNA detection and imaging in living cells. Anal Chim Acta 1063:152-158

[30] Yan X, Song Y, Zhu CZ, Li HX, Du D, Su XG, et al (2018) MnO_2 nanosheet-carbon dots sensing platform for sensitive detection of organophosphorus pesticides. Anal Chem 90:2618-2624

[31] Mo Z, She XJ, Li YP, Liu L, Huang LY, Chen ZG, et al (2015) Synthesis of $g-C_3N_4$ at different temperatures for superior visible/UV photocatalytic performance and photoelectrochemical sensing of MB solution. RSC Adv 5:101552-101562

[32] Cai Y, Fang JK, Wang BF, Zhang FS, Shao G, Liu YJ (2019) A signal-on detection of organophosphorus pesticides by fluorescent probe based on aggregation-induced emission. Sensor Actuat B-Chem 292:156-163

[33] Lin XF, Yu QR, Yang W, He CX, Zhou Y, Duan N, et al (2021) Double-enzymes-mediated fluorescent assay for sensitive determination of organophosphorus pesticides based on the quenching of upconversion nanoparticles by Fe^{3+}. Food Chem 345:128809

[34] Tan L, Guo ML, Tan JA, Geng YY, Huang SY, Tang YW, et al (2019) Development of high-luminescence perovskite quantum dots coated with molecularly imprinted polymers for pesticide detection by slowly hydrolysing the organosilicon monomers in situ. Sensor Actuat B-Chem 291:226-234

[35] Huang N, Qin YF, Li M, Chen TX, Lu MJ, Zhao JJ (2019) A sensitive fluorescence assay of organophosphorus pesticides using acetylcholinesterase and copper-catalyzed click chemistry. Analyst 144:3436-3441

[36] Lin BX, Yan Y, Guo ML, Cao YJ, Yu Y, Zhang TY, et al (2017) Modification-free carbon dots as turn-on fluorescence probe for detection of organophosphorus pesticides. Food Chem 245:1176-1182

[37] Bhamore JR, Ganguly P, Kailasa SK (2016) Molecular assembly of 3-mercaptopropinonic acid and guanidine acetic acid on silver nanoparticles for selective colorimetric detection of triazophos in water
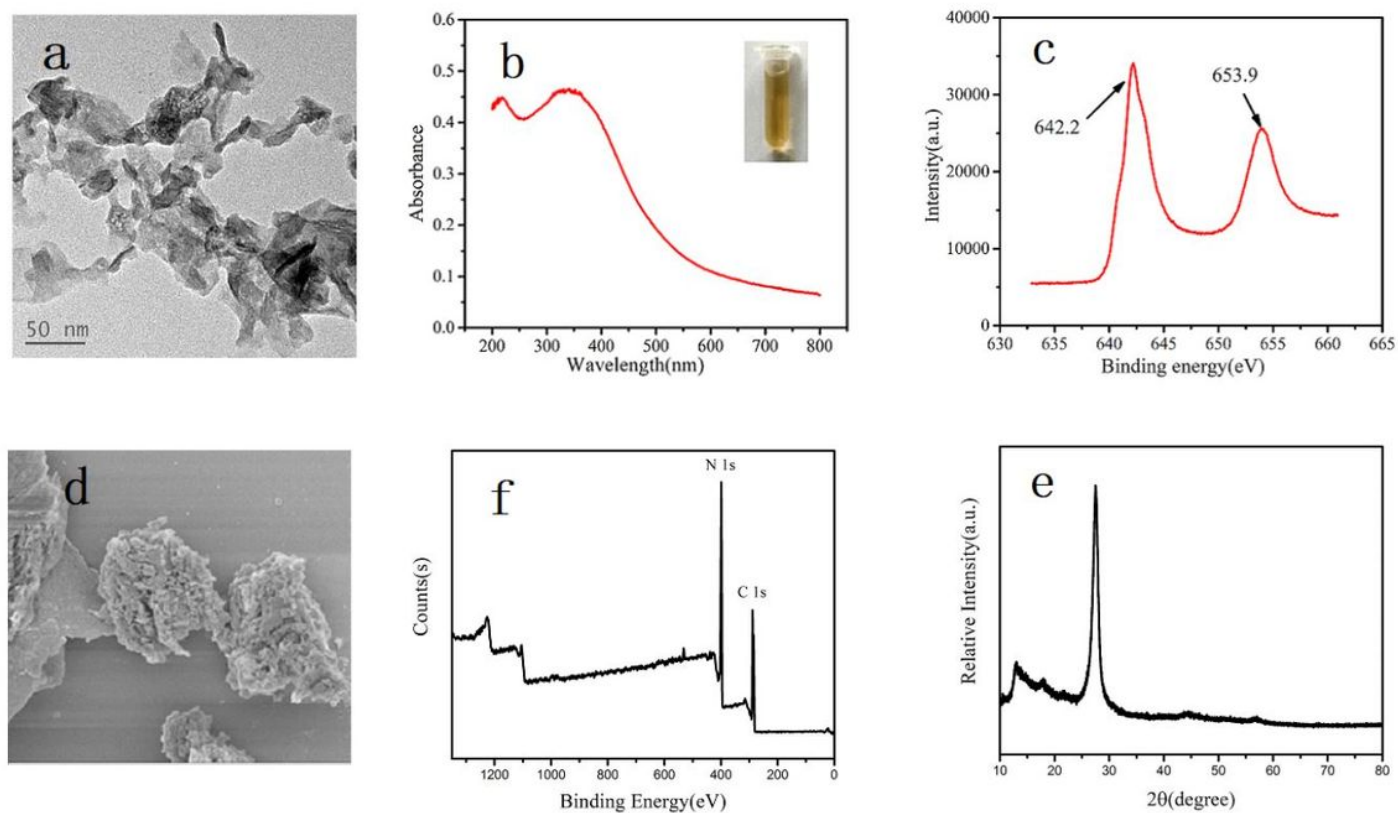
and food samples. Sensor Actuat B-Chem 233:486-495

Figures

Figure 1

(a) TEM image of MnO2 NS, (b) UV–vis absorption spectra of MnO2 NS, inset: digital image of MnO2 NS and (c) XPS spectra of MnO2 NS, (d) SEM images of g-C3N4, (e) XPS spectra of g-C3N4, (f) survey XPS spectra of g-C3N4
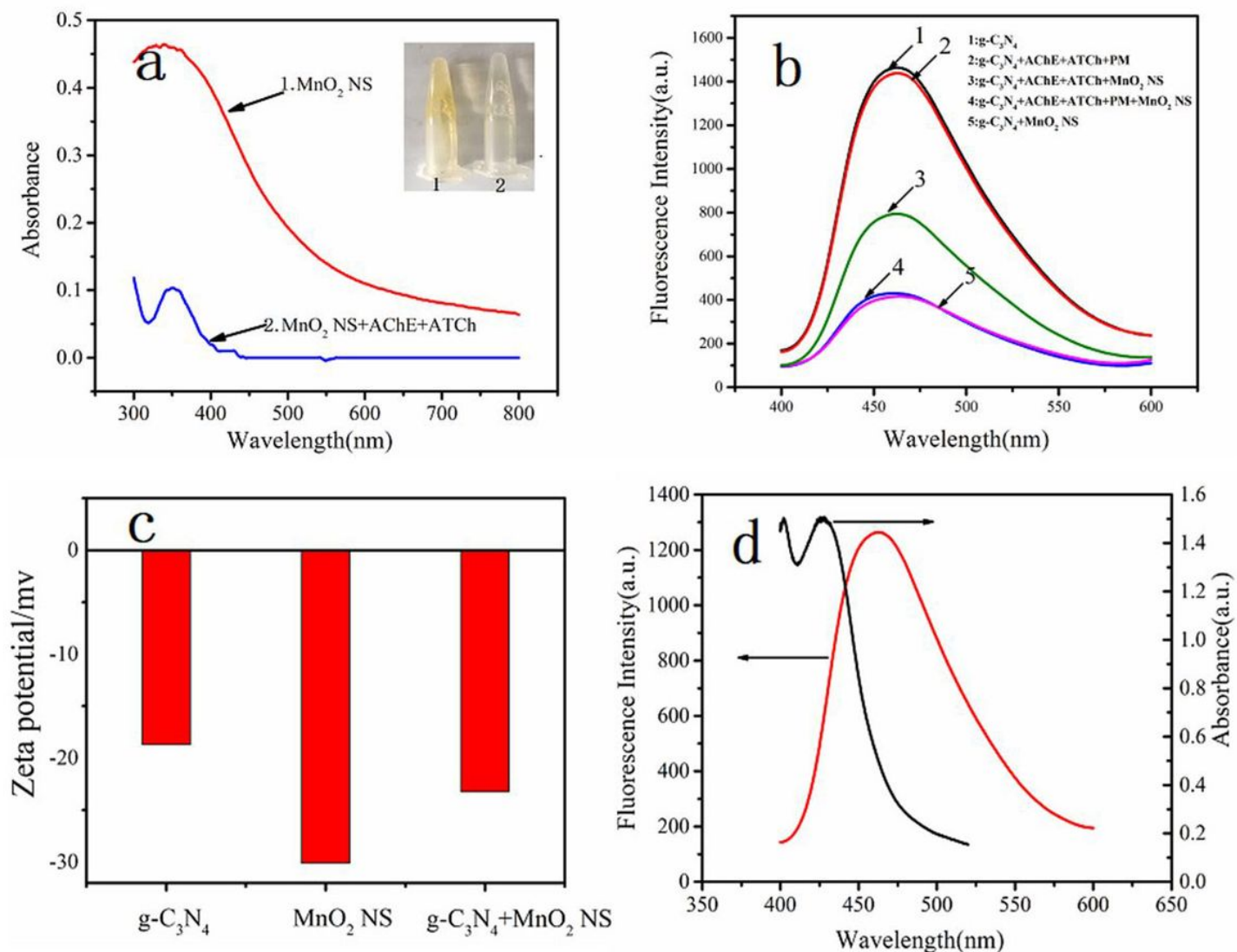
Figure 2

(a) UV-vis absorption spectrum of (1) MnO2 NSand (2) MnO2 NS+AChE+ATCh, inset: the corresponding photos; (b) Fluorescence spectra of g-C3N4 and the mixture with different substances; (c) Zeta-potentials of MnO2 NS, g-C3N4, and MnO2 NS+ g-C3N4; (d) The fluorescence spectra of g-C3N4 and the absorption spectra of MnO2 NS
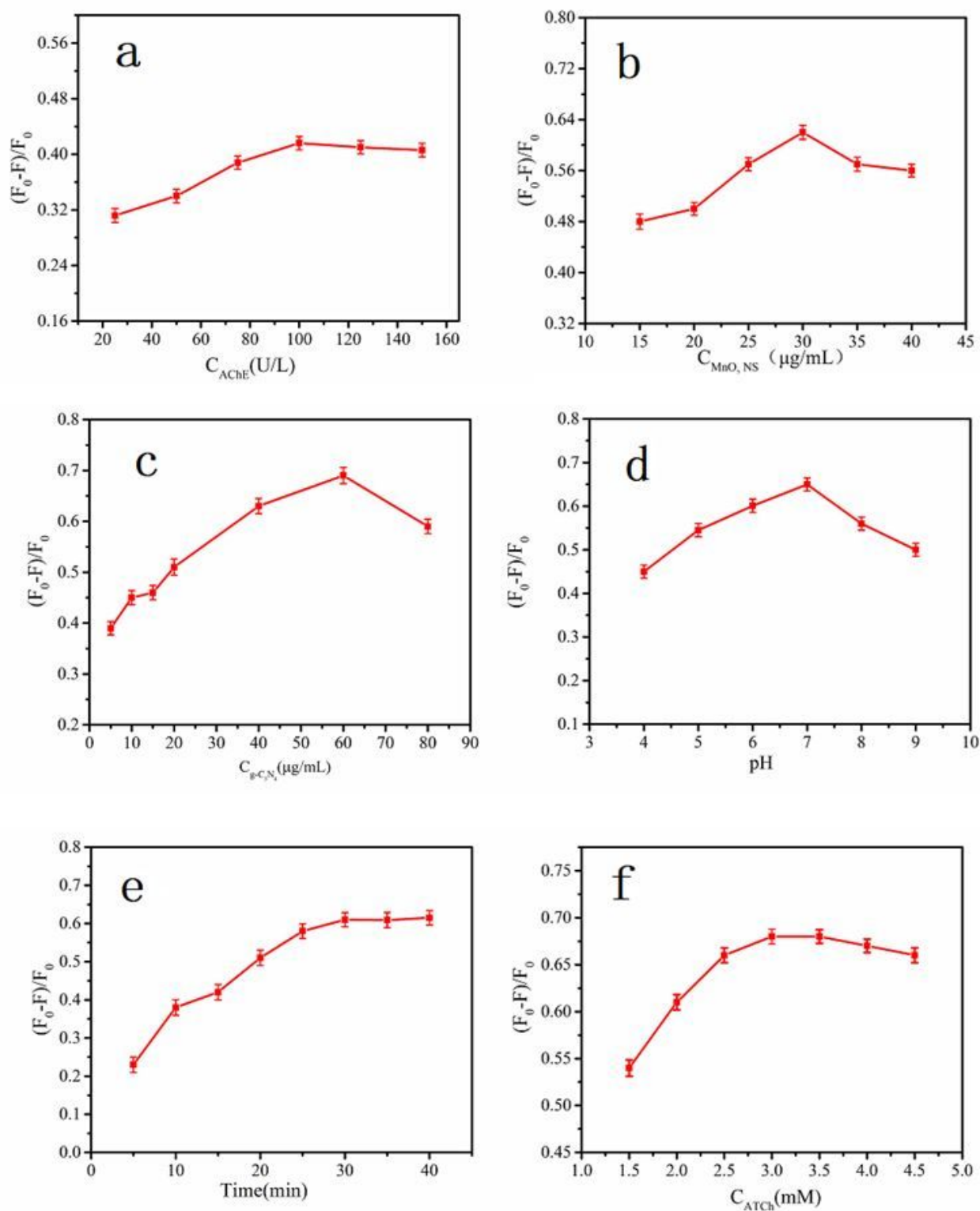
Figure 3

The effect of the concentrations of AChE (a), MnO2 NS (b) and g-C3N4 (c), pH (d), the reaction time (e), and the concentration of ATCh (f) on the relative intensity
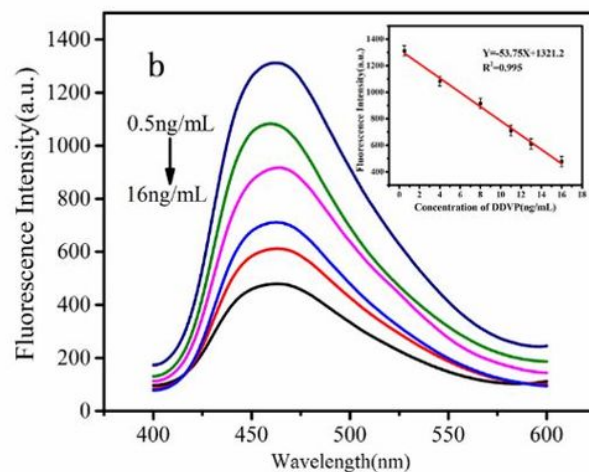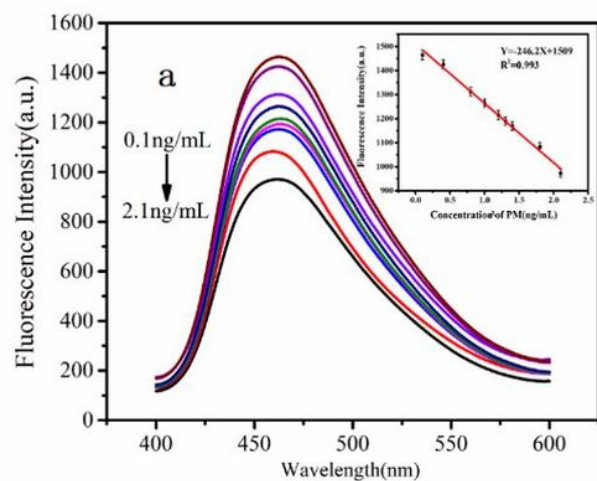
Figure 4

Sensitivity for determination of (a) PM (from up to down: 0.1, 0.4, 0.8, 1, 1.2, 1.4 1.8, 2.1 ng/mL) and (b) DDVP (from up to down: 0.5, 4, 8, 11,13 and 16 ng/mL), inset: calibration curve for PM and DDVP, respectively.
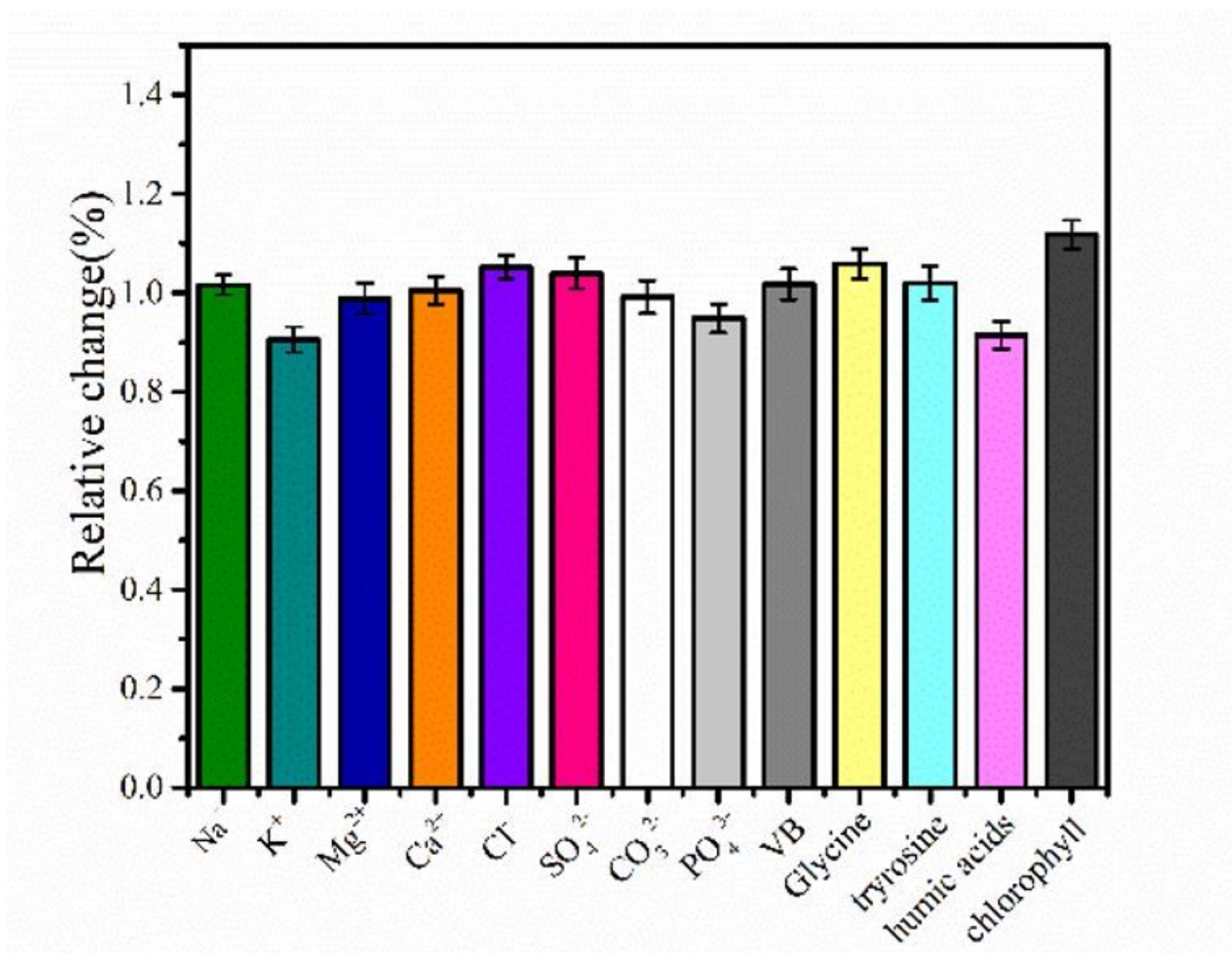
Figure 5

The selectivity of proposed method.

Supplementary Files

This is a list of supplementary files associated with this preprint. Click to download.

- scheme1.jpg